A Dielectric Resonator Fed Wideband Metasurface Antenna With Radiation Pattern Restoration Under Its High Order Modes

YONGHUI QIU[1], ZIBIN WENG[1], (Senior Member, IEEE),
ZHI-QIANG ZHANG[2], JIANFENG LIU[1], HONG-WEI YU[1],
AND YI-XUAN ZHANG[1], (Graduate Student Member, IEEE)
[1]National Key Laboratory of Antennas and Microwave Technology, Xidian University, Xi'an 710071, China
[2]Northwest Institute of Nuclear Technology, Xi'an 710024, China

Corresponding author: Zibin Weng (zibinweng@mail.xidian.edu.cn)

ABSTRACT In this article, a dielectric resonator (DR) excited wideband metasurface (MTS) antenna with differential feeding is proposed, which uses two modes of the MTS and the fundamental mode of the DR to achieve multimode operation and obtain wide bandwidth. Initially, based on the characteristic mode theory, relevant modes of the MTS are analyzed. Then, a DR operating at the fundamental mode ($\text{TE}^x_{\delta 11}$) is introduced as the magnetic current source to feed the MTS, exciting the dominant mode and high order mode (HOM) of the MTS simultaneously. However, this HOM has a weak gain at the broadside direction and large side lobes. According to the superposition principle of radiation patterns, the maximum at the broadside generated by the DR is utilized to enhance the boresight gain of the HOM, thus transforming the top-weak radiation pattern of this HOM into a broadside one and improving the gain flatness. Additionally, the differential feeding technique is introduced to improve the asymmetry of radiation pattern. Furthermore, by analyzing the out-of-phase currents and the periodicity of the MTS patches, three measures —loading transverse open-ended slots, shortening periodicity and loading longitudinal slots— are introduced to reduce the high side lobe level of the HOM while preserving radiation patterns undistorted and improving the gain stability. As a result, this HOM and the dominant mode of the MTS are combined with the fundamental mode of the DR, achieving multimode operation. Finally, the proposed antenna was fabricated and measured. The measured results agree well with the simulated ones, indicating an impedance bandwidth of 51.4% (4.38-7.41 GHz), a 5-9 dBi in-band gain and a 15 dB front-to-back ratio (FBR) within the operating band.

INDEX TERMS Dielectric resonator antenna, metasurface, wideband, high order mode, radiation pattern restoration.

I. INTRODUCTION

Wideband working is a vital antenna characteristic required by a wide range of applications. Recently, many methods have been proposed to broaden antenna impedance bandwidth [1]–[6]. Loading metasurface (MTS) is one of the effective ways, due to its merits of low profile and multi-modes operation [7], [8]. Besides, MTS, as a two-dimensional metamaterial, has been increasingly investigated in other fields including polarization conversion [9], frequency selection surface [10], broadband decoupling [11] and end-fire antenna [12].

The associate editor coordinating the review of this manuscript and approving it for publication was Lu Guo[ID].

To satisfy the demand of wideband wireless communication systems, it is necessary to explore new methods to improve the bandwidth of metasurface antenna (MA). MA usually requires an external antenna as the feed source to provide a stable excitation. Then MTS and the feed form a combined radiator, achieving a multimode wideband property. Therefore, for a better working bandwidth, both a wideband feed source and a MTS with multi resonances are indispensable.

On the one hand, the feeding structure can be improved for bandwidth enhancement. At present, a microstrip coupling slot is typically adopted to excite MTS [13], [14], owing to the advantages of low profile and wide working bandwidth. However, it is inevitable to suffer from the strong back radiation,

due to the slot on the ground. Moreover, it has recently emerged a kind of CPW fed slot to couple MA in [15], which still uses the slot to excite MTS and has a large back lobe. As a result, to avoid the strong back radiation of slot coupling, some feeding mechanisms, such as the suspended dipoles [16], coaxial cable [17] and coplanar dipoles [18], have been proposed to feed MTS, achieving 24%, 36% and 45% working bandwidth, respectively. Besides, a patch-coupled MA [7], with a 30% bandwidth, uses the TM_{10} mode of the patch to feed MTS. However, the patch antenna has an intrinsically narrow mode bandwidth, which limits its potential as a wideband feeding source. In our previous report in [19], a DR fed MA achieves a bandwidth of 30% by simultaneously exiting the fundamental mode of the DR and the in-phase dominant mode of the MTS. However, its bandwidth is not wide enough due to its unavailable HOM of the MTS, which is important for the further extension of the operating bandwidth in the higher frequency.

Generally, with regard to feeding structure, limited bandwidth and strong back radiation still remain to be improved.

On the other hand, the multi-modes characteristic of MA, which has enormous potentials, still remains to be further exploited. Due to their distorted radiation patterns and deteriorated polarization purity, high order modes (HOMs) of MA are less investigated compared with the dominant mode. Recently, HOMs of MA in [14] and [18] are directly used to broaden the antenna working bandwidth because both of them are inherently broadside. A MA with a conical radiation pattern is studied in [20] for omnidirectional application. A radiation null is caused at broadside due to HOM. Therefore, it is necessary to further study how to reshape and apply HOMs with distorted radiation patterns for the broadside radiation bandwidth enhancement.

In summary, a majority of slot coupled MA can realize wide bandwidth but have large back lobes, while other feeding methods avoid the strong back radiation but still bear limited bandwidth. Furthermore, HOMs with distorted radiation patterns need to be reshaped to further broaden the bandwidth of MA. Therefore, it is challenging to design a novel wideband feeding structure with reduced back radiation and to use distorted HOMs to further enhance the bandwidth.

In this article, by using the dielectric resonant (DR) as a feeding source, a wideband MA is proposed, which uses the fundamental mode of the DR, the dominant mode and the HOM of the MTS to realize multimode operation for broad bandwidth. Noting that the HOM of the MTS has a weak gain at the broadside direction. In order to obtain a wide bandwidth and a reduced back radiation, a rectangular DR which has a wide mode bandwidth and high design flexibility, is introduced as the feeding structure for the MA. Thus, both the dominant mode and the differential mode of the MTS are excited simultaneously. Meanwhile, the top-weak radiation pattern of the HOM is transformed into broadside radiation, resulting in a stable broadside radiation over wide working band. Then, the asymmetry of radiation attributed to the deviating inner field of DR is improved by the differential

feeding structure. Moreover, to suppress high side lobe level while maintaining an undistorted radiation pattern and stable gain, three measures—loading transverse open-ended slots, shortening periodicity and loading longitudinal slots—are introduced, leading to a significantly reduced side lobe level and substantially mitigated gain fluctuation. These radiation reshaping methods may also be applied to other HOMs to realize fruitful functions. Finally, broad bandwidth with multi-mode operation and stable broadside radiation is realized by the proposed antenna while maintaining low back radiation.

II. ANTENNA CONFIGURATION

Fig. 1 shows the configuration of the proposed antenna, which consists of a rectangular DR mounted on the ground, the surrounding patches and a feeding network at the bottom substrate. The DR (Al_3O_4), which has a relative permittivity of $\varepsilon_{r1} = 9.5$, a loss tangent of $\tan\delta = 0.001$ and a size of $a \times b \times d$, is fed by a pair of differential probes. The probe, with height h_0 and diameter d_0, is soldered to a rectangular metal strip. The rectangular metal strip, which has a height of h_1 and a width of d_1, is attached to the side face of the DR. The MTS comprises an array of 4×3 patches with a period of p_y and a gap of g_y in the y-direction, while the corresponding parameters along the x-direction are p_x and g_x, respectively. The size of the rectangular patch in the x-direction and y-directions are l_x and l_y, respectively. The circumscribed length of patches in the x and y-direction are w_{sqx}, w_{sqy}, respectively. For the placement of DR, the two central patches and the corresponding region of the substrate are removed. With a space p_1 from the central line, the transverse open-ended slots, which have a length of s_1 and a width of w_1, are loaded at four flank patches. Four longitudinal slots, which are positioned at the central line of each patch, split four corner patches, respectively. Both the upper substrate and lower substrate are made of F4B (relative permittivity $\varepsilon_{r2} = 3.5$, loss tangent $\tan\delta = 0.001$) with a size of $w \times w$. The detailed variables of the final prototype are listed as follows (Units: mm): $a = 14.1$, $b = 8.3$, $d = 8.3$, $h_0 = 2.5$, $d_0 = 0.5$, $h_1 = 7$, $d_1 = 0.2$, $h = 4$, $t = 0.5$, $w = 52$, $p_y = 7.6$, $g_y = 1.1$, $p_x = 9$, $g_x = 0.8$, $l_y = 6.5$, $l_x = 8.2$, $s_1 = 3.4$, $w_1 = 0.2$, $p_1 = 5.4$, $w_2 = 0.5$, $w_{sqy} = 29.3$, $w_{sqx} = 26.2$.

III. WIDEBAND OPERATING PRINCIPLE
A. THE CHARACTERISTIC MODE ANALYSIS OF SOURCE-FREE MTS

The theory of Characteristic mode (TCM) provides clear physical insights on the mode behaviors of antennas, which is helpful in understanding the underlying radiation mechanism and designing antenna. Thus, characteristic mode analysis (CMA) has been increasingly used to guide MA design for various applications in recent years [21]–[23].

According to the empirical design formulas in [13], we figure out the initial size of elemental square metal patch based on the proposed center frequency (6 GHz) as follows
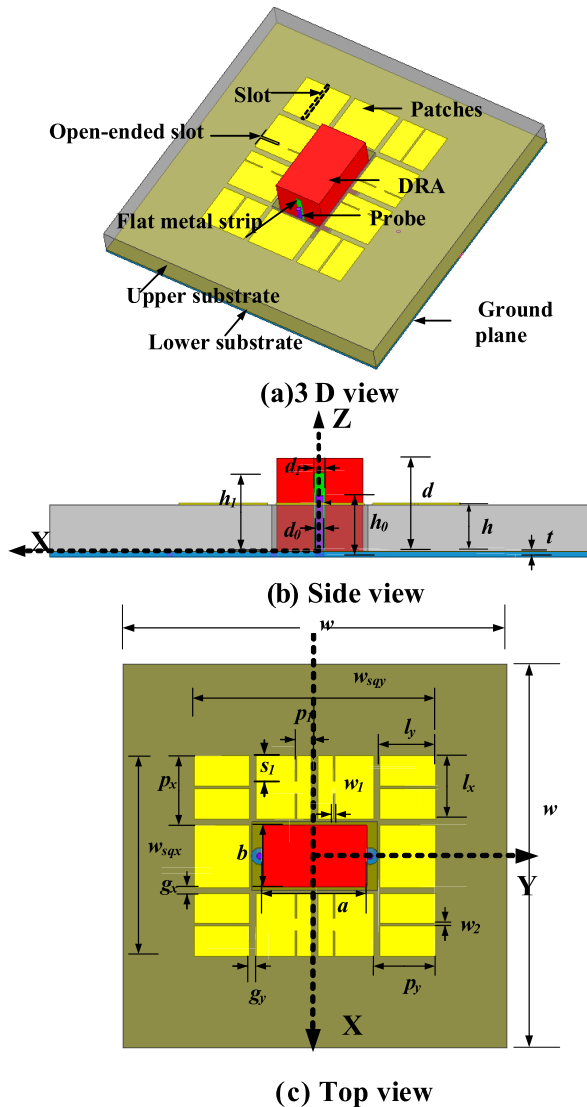
(a) 3 D view

(b) Side view

(c) Top view

FIGURE 1. Configuration of the proposed antenna.

(Units: mm): $p_x = p_y \approx 13.4$, $g_x = g_y \approx 1$, where each patch has a length of $\frac{1}{2}\lambda_d$ (λ_d is the dielectric wavelength). Accordingly, the 3×3 patches, which has a circumscribed length (w_{sqy}) of $\frac{3}{2}\lambda_d$, operates at the Q-TM$_{30}$ mode.

Based on [24], the DR working at the TE$^x_{\delta 11}$ mode can be equivalent to a magnetic current source. And it is the sufficient coupling strength provided by the magnetic source that guarantees the excitation of the desired modes. Thus, it is important to strengthen the coupling coefficient between the magnetic current source (DR) and the patches. Besides, the subsequent placement of the DR should also be taken into consideration. Therefore, the MTS are cut into 4 patches in the y direction at the fixed w_{sqy}, forming a gap between the two central rows of patches. Then, the magnetic current source can be centered below the gap, which can bring in a better coupling coefficient. Meanwhile, the patch size is shortened ($p_x = p_y = 10.1$ mm, $g_x = g_y = 0.8$ mm), thus the region of two central patches make enough room for placing the DR. Moreover, because the patch size (p_x) is comparative

to the width of the DR ($b = 8.3$ mm), the number in the x-direction is preserved as 3 to achieve a compact size and better coupling coefficient.

As a result, the configuration of the MTS is formed as shown in the Fig. 2. Then, the following CMA is performed on this configuration.

With reference to [25], the characteristic mode analysis of the source-free MTS is carried out using multilayer solver of CST Microwave Studio (MWS). Fig. 2 shows the first ten characteristic modes. Based on the TCM in [25], the first 10 modes can be classified into 5 pairs of orthogonal modes, where each mode in every pair is orthogonal to the other one in terms of both the amplitude and orientation. As can be seen from Fig. 2, we can conclude that the 5 pairs of orthogonal modes as follows: $J_1 \& J_2$, $J_3 \& J_5$, $J_4 \& J_6$, $J_7 \& J_8$, $J_9 \& J_{10}$, where the two modes of one pair have similar characteristics.

Initially, we discuss the unwanted modes. Both the J_3 and J_5 mode have a split beam due to their anti-phase currents. While the J_4 and J_6 mode have a radiation null at the broadside direction. As for the J_7 and J_8 mode, their radiation patterns bulge at four corners while boresight directivity is nearly zero. If the J_3-J_8 mode are unfortunately excited, a large gain fluctuation within operating band will be inevitable. Therefore, the J_3-J_8 mode are unwanted modes.

Then, the desired modes are analyzed as follows: Firstly, the J_1 and J_2 mode have in-phase current and broadside radiation. Secondly, though J_9 and J_{10} have anti-phase currents distribution, the beam at the boresight direction can also be observed. Therefore, the J_1, J_2, J_9 and J_{10} mode are the desired modes.

Besides, the J_1 (J_2) and J_9 (J_{10}) mode have the same y (x)-polarization and the broadside radiation, though the main beam of J_9 is weaker compared with its large side lobes. Thus, excitation of either one of the two combinations, which are the pair of $J_1 \& J_9$ mode or the group of $J_2 \& J_{10}$ mode, will lead to a linear polarization, wide bandwidth and broadside radiation. Considering the placement of the rectangular DR, here we take the J_1 and J_9 mode for example.

In addition, the modal significance in Fig. 3 exhibits that J_1 and J_9 resonant at 5.52 and 6.42 GHz, respectively. Thus, to excite the two modes, the operating band of the magnetic current source should be wide enough and be finely adjusted to cover the resonances of the J_1 and J_9 mode.

B. THE FEEDING MECHANISM FOR WIDEBAND OPERATION

It is well known that the magnetic current source can be represented by a slot on ground plane, which usually has a large back lobe. With reference to [24], the DR operating at the TE$^x_{\delta 11}$ mode can also be equivalent to a magnetic current, serving as an effective magnetic current source without etching a slot on the ground. Thus, the back radiation can be reduced by using this new feeding structure.

With reference to TCM, the modal weighting coefficients (MWCs) (α_n) represent the proportion of mode J_n in the total
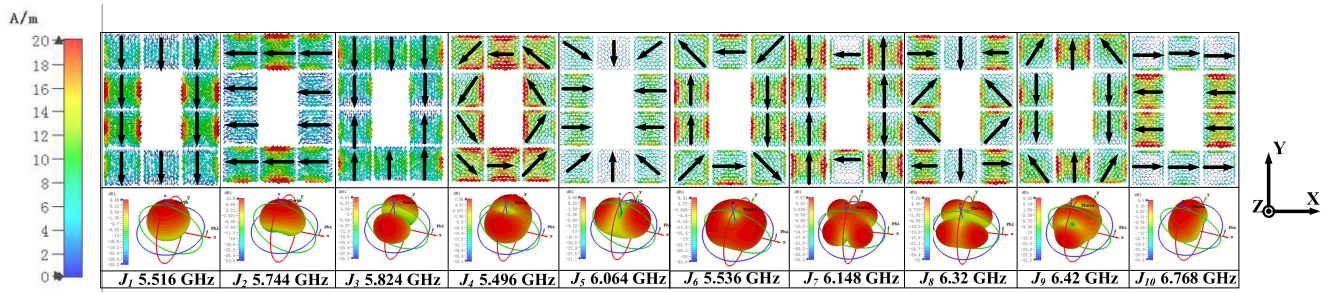
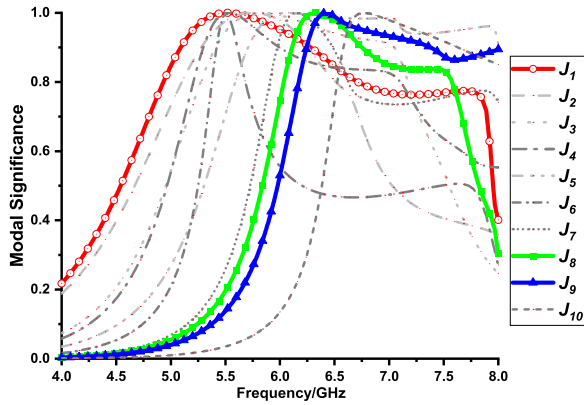**FIGURE 2.** Modal currents and modal radiation patterns of first ten modes.

FIGURE 3. Modal significance of the MTS.

currents as defined by [26]

$$\alpha_n = 1/(1 + j\lambda_n) \int J_n \bullet E_i dS \qquad (1)$$

where λ_n is the eigenvalue of mode J_n, E_i is the external E-field from feeding source, and s is the surface of conductor area. The first term in the equation is the modal significance (MS), and the second term is named modal excitation coefficient (MEC), which are defined as

$$MS = 1/|1 + j\lambda_n| \qquad (2)$$

$$V_i = \int J_n \bullet E_i dS \qquad (3)$$

It can be found that the undesired modes can be suppressed by reducing the $|V_i|$. The feeding source DR operating at the $TE^x_{\delta 11}$ mode can be equivalent to a magnetic current along the x-axis, which provides the E-fields component in the y-direction. Thus, for an impressed E-field E_y provided by the DR, only the J_1 and J_9 mode are well excited due to the same polarization as the feeding source DR. The rest of modes J_2, J_4, J_5-J_8 and J_{10} have the J_x (the current component along the x-axis), so these modes will not be excited due to the polarization orthogonality. As for the J_3 mode, though it has the same polarization as the feeding (DR), it still has little potential to be excited. This is due to the factor that the $TE^x_{\delta 21}$ mode of DR, which has out-of-phase inner E-fields and may excite the J_3 mode with the anti-phase currents along the y-axis, has been excluded out of our proposed working band.

As a result, under the coupling fields of DR, only J_1 and J_9 mode can be successfully excited.

Moreover, compared with the patch antenna, the DR is a better feeding source for the MTS, since it has a wider mode bandwidth to excite the MTS stably. Based on the dielectric waveguide model (DWM) in [27], we can figure out the $TE^x_{\delta 11}$ and $TE^x_{\delta 21}$ mode of our DR operates at 5.6 GHz and 8.4 GHz, respectively, which are consistent with the simulated E-fields distribution depicted in Fig. 4. Thus, it is clear that the fundamental mode ($TE^x_{\delta 11}$) has a wide bandwidth, representing a wide enough interval between the $TE^x_{\delta 11}$ mode and $TE^x_{\delta 21}$ mode. Because of the out-of-phase inner E-fields distribution (Fig. 4 (b)), the $TE^x_{\delta 21}$ mode of DR should be avoided in the feeding usage.
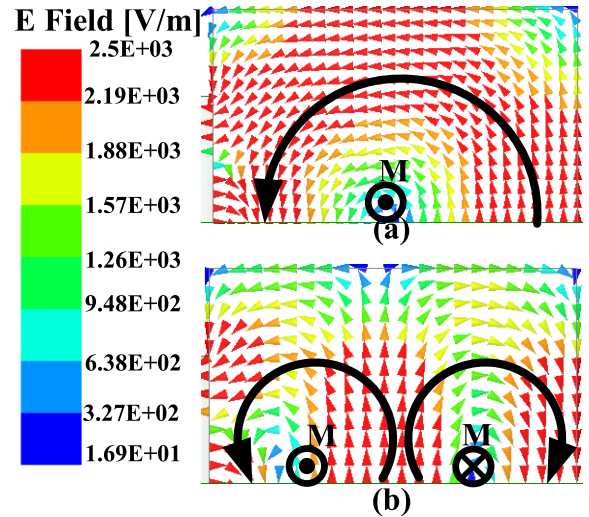

FIGURE 4. E-fields of DR: (a) $TE^x_{\delta 11}$ mode at 5.6 GHz; (b) $TE^x_{\delta 21}$ mode at 8.4 GHz.

Additionally, in order to cover the J_1 and J_9 mode, avoid the $TE^x_{\delta 21}$ mode and obtain the maximum bandwidth, the operating band needs a fine adjustment. Thanks to the three-dimensional structure, DR is more flexible in design than other kinds of antennas, which is helpful in adjusting the size of DR to allocate operating band.

More importantly, as demonstrated in Fig. 5, it is the broadside radiation from DR that transforms the top-weak radiation pattern of the J_9 mode into broadside radiation. As observed from CST MWS, the J_9 mode has a 6.6 dB directivity at the

boresight while its side lobe has a level of 8.8 dB. Meanwhile, the DR operating in the $TE_{\delta 11}^x$ mode generates a maximum at the broadside, which enhances the weak radiation of the J_9 mode at the broadside direction. So the J_9 mode can also contribute to the broadside radiation, expanding bandwidth at the high-frequency band. Thus, a wideband performance with tri-modes operation consisting of the $TE_{\delta 11}^x$ mode of DR, the dominant mode J_1 and HOM J_9 of the MTS are formed. In other words, the DR is not only a feeding structure but also an indispensable constituent part of multimode wideband.
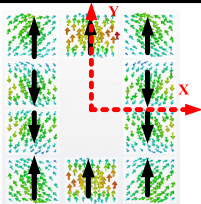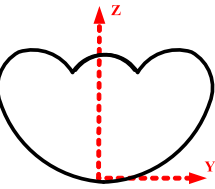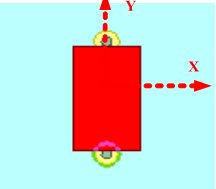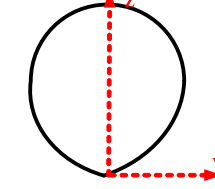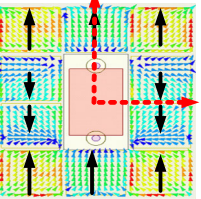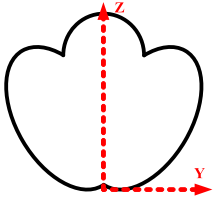
FIGURE 5. Radiation patterns of three distinctive antennas.

IV. RADIATION PATTERN RESTORATION

The radiation pattern distortion of the proposed antenna can be classified into two parts, including the E-plane asymmetry resulting from the transitional mode ($TE_{\delta 1+\delta 1}^x$) of DR and the high side lobe level caused by the J_9 mode of the MTS.

As demonstrated in Fig. 6 (a), under the transitional mode ($TE_{\delta 1+\delta 1}^x$) between the $TE_{\delta 11}^x$ and $TE_{\delta 21}^x$ mode, the equivalent magnetic current of the DR deviates from the x-axis, thus deteriorating the symmetry of radiation in the E-plane. As shown in Fig. 6, by employing differential feeding, the equivalent magnetic current of DR can be stabilized at the x-axis, thus the asymmetry is modified.

The high side lobe level in E-plane under the J_9 mode should be attributed to the out-of-phase current distribution across the MTS patches. So we investigate the relative magnitude of out-of-phase currents and the periodicity of the MTS patches, which play key roles in the high side lobe level. Then, three measures—loading transverse open-ended slots, shortening periodicity and loading longitudinal slots—are introduced to improve radiation patterns and gain
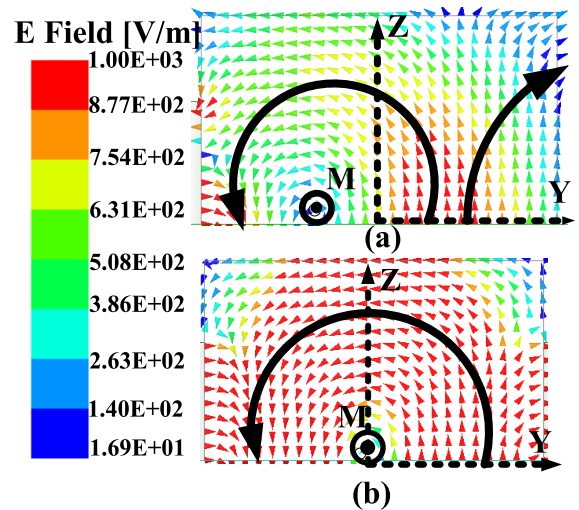
FIGURE 6. E-fields of transitional DR under transitional mode: a) single probe feeding; b) differential probe feeding.
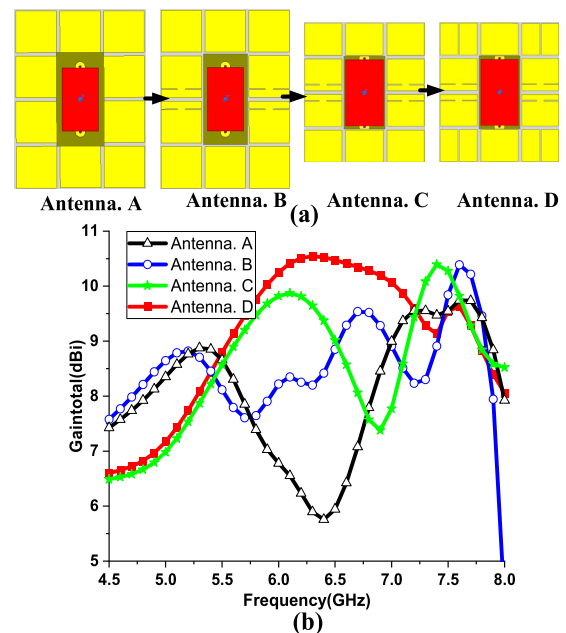
FIGURE 7. Evolution of antenna: (a) evolution of antenna configuration; (b) gain improvement of antennas.

stability. As shown in Fig. 7, the configuration of the antenna evolves. The in-band fluctuation of boresight gain is gradually improved. Meanwhile, the side lobe level is gradually reduced. It is noted that the period in the y-direction (p_y) is shortened while the x-oriented period (p_x) is remained unchanged during the evolution.

A. MODELING ANALYSIS OF KEY PARAMETERS FOR SIDE LOBE LEVEL REDUCTION

From the previous analysis, we can conclude that it is the out-of-phase currents of the MTS under the J_9 mode that cause the high side lobe level in the E-plane. Since the high side lobe level only occurs in the E-plane, the radiation pattern of the E-plane is investigated independently.

To simplify the analytical model and focus on the key parameters, we decompose the currents of the MTS into four parts along the *E*-plane (y-direction) which are represented by the four rows of patches. As depicted in Fig. 8, each row of patches provides $+y$ or $-y$-component of current. Thus the four collinear parts form a four-element array. The currents component at $\pm 3/2p$ and $\pm 1/2p$ are marked as J_1, J_2, J_3 and J_4, where J_1 and J_4 (J_2 and J_3) have the same amplitude $\alpha(\beta)$ and phase, because of the symmetry in antenna structure. And the J_1 (J_4) is out of phase with J_2 (J_3). Thus, the array factor $F(\theta)$ can be expressed as

$$F(\theta) = \alpha e^{-jk\frac{3}{2}p\sin\theta} + \alpha e^{jk\frac{3}{2}p\sin\theta} - \beta e^{-jk\frac{1}{2}p\sin\theta} - \beta e^{jk\frac{1}{2}p\sin\theta}$$
$$= 2\alpha\cos(k\frac{3}{2}p\sin\theta) - 2\beta\cos(k\frac{1}{2}p\sin\theta) \quad (4)$$

According to formula (4), the key factors of controlling radiation patterns are the relative amplitude of currents $\alpha(\beta)$ and periodicity of the MTS patches p (element space p). Here, the p of formula (4) represents the period of patches in the y direction (p_y). Based on formula (4), the effect of current relative magnitude and periodicity of the MTS patches on side lobe level reduction is demonstrated in Fig. 9. It can be seen from Fig. 9 that the high side lobe level in the *E*-plane can be reduced with the decrease of out-of-phase currents relative magnitude β or the MTS patches periodicity p in the y-direction (*E*-plane). Therefore, we use the above conclusions of model analysis to reform the MTS, thus performing the reduction of high side lobe level. Then, the validity of the above modal analysis and operation on the radiator is verified by full-wave simulation.
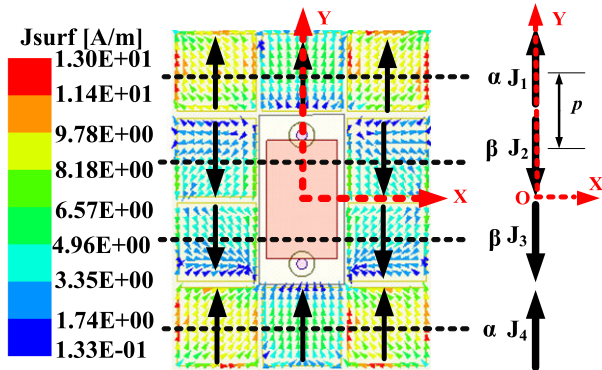

FIGURE 8. Sketch of equivalent model.

B. LOADING TRANSVERSE OPEN-ENDED SLOTS

The above analysis indicates that the side lobe level can be reduced by suppressing the relative magnitude of out-of-phase currents. So the transverse open-ended slots are loaded on four flank patches to reduce anti-phase currents, which can lower the relative magnitude of anti-phase currents. As shown in Fig. 10(c), the transverse open-ended slots should be located at the position with the strongest currents magnitude distribution, thus reducing the majority of out-of-phase currents. Also, the open-ended slots are recommended to be long and thin, resulting in most currents to flow around slots.
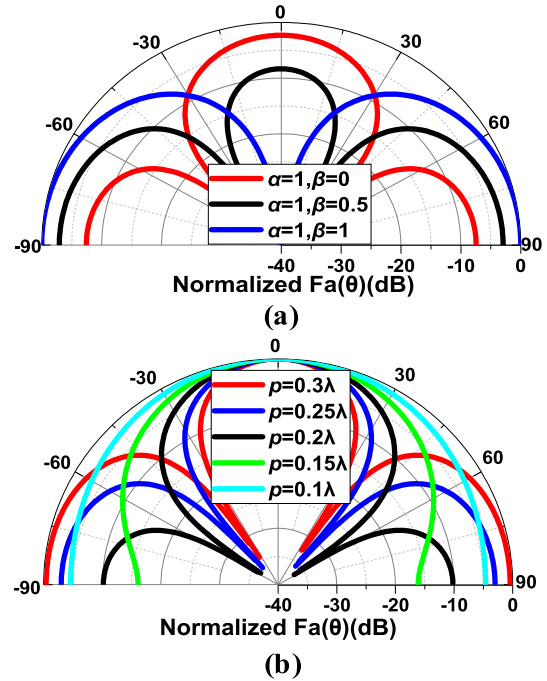

FIGURE 9. Normalized patterns of the array factor at the *E*-plane (b) with different values of β under $p = \lambda/4$; (c) with different values of p under $\alpha = 1$ and $\beta = 0$.

As shown in Fig. 10(c), the slots should be thin enough so that the opposite currents on both sides are close enough to cancel each other out in the far field. And the slots are recommended to be long enough so that the reverse currents on the patch can be reduced adequately. As can be seen from Fig. 10(a), (b) and Fig. 11(b), as open-ended slots length s_1 increases, the current magnitude difference between central flank patches and side patches is increasingly obvious, which indicates that relative magnitude β of out-of-phase currents can be weakened by loading transverse open-ended slots.
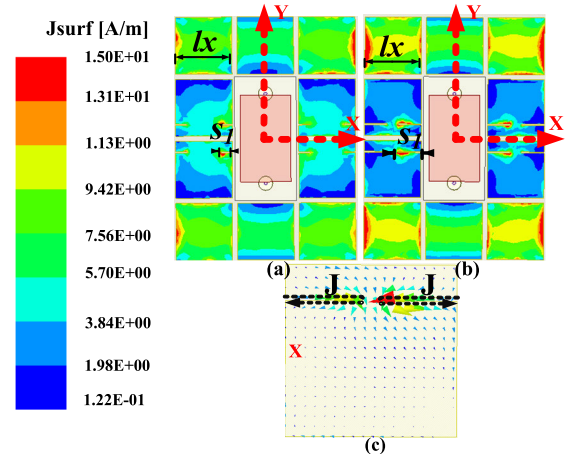

FIGURE 10. Schematic of open-ended slots: magnitude of current distribution under the J_9 mode (a) $s_1/l_x = 0.2$; (b) $s_1/l_x = 0.4$; (c) vector of current distribution with slots.

However, it is challenging to determine the proper location of the transverse open-ended slots. This is due to the factor that we need to suppress the out-of-phase currents of high

order mode J_9 while minimizing the side effect on the dominant mode J_1. Hence, the optimum position of loading slots is investigated. As shown in Fig. 11(a) and (b), compared with the J_1 mode, the position of strongest out-of-phase currents on central flank patches under J_9 mode is closer to the *x*-axis. So the transverse open-ended slots should be located at the position near the *x*-axis on the flank patches.
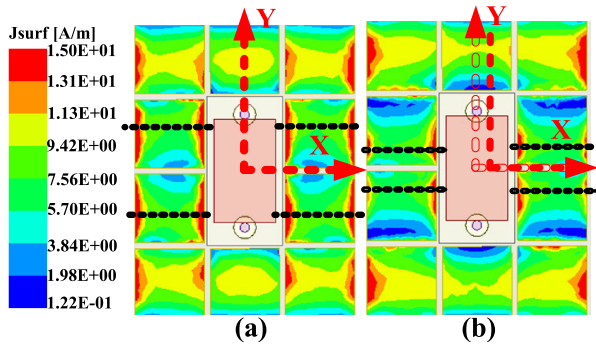

FIGURE 11. Magnitude distribution of currents on the MTS in Antenna. A (a) without slots under J1 mode; (b) without slots under J9 mode.

Simulated results in Fig. 12 (a) exhibit that the side lobe level is significantly reduced as the transverse open-ended slots length increase (the flank patches can't be completely cut off), thus verifying the above model analysis of loading transverse open-ended slots.
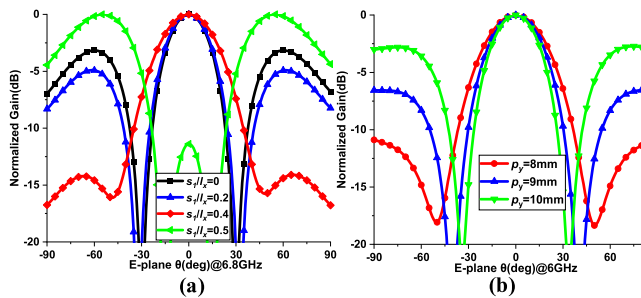

FIGURE 12. Simulated radiation patterns at E-plane: (a) with different values of slot length at 6.8 GHz; (b) with different values of period in the E-plane at 6 GHz.

C. SHORTENING PERIODICITY OF THE MTS IN THE E-PLANE

Due to the transverse open-ended slots, the high side lobe level under the high order mode J_9 has been effectively suppressed, thus contributing to a significant recovering in boresight gain under J_9 mode and a moderate in-band gain fluctuation (Fig. 7 (b) from Antenna. A to Antenna. B).

However, the open-ended slots have no consistent effect on boresight gain over the entire broadband. From Fig. 7 (b) (Antenna .B), a collapse in boresight gain around 6 GHz still remains to be solved. It is worth noting that the periodicity of the MTS patches (Antenna .B) in the E-plane p_y (10mm) is 0.2 wavelength under 6 GHz. Consequently, according to modal analysis from formula (4) and Fig. 9(b), the periodicity in the *y*-direction (p_y) should be shortened based on

Antenna. B to further suppress the side lobe level and mitigate the gain fluctuation. Simulated results in Fig. 12(b) and Fig. 7(b) indicate that side lobe level is reduced and boresight gain at 6 GHz is recovered.

D. LOADING LONGITUDINAL SLOTS

As shown in Fig. 7(b), after loading transverse open-ended slots and shortening the periodicity of the MTS patches, the gain collapse at the middle frequency (6 GHz) is improved to a normal level and the in-band gain flatness is substantially improved.

Nevertheless, the boresight gain around 7 GHz falls back (Fig. 7(b)). By comparing currents distribution of the MTS at 7 GHz with the J_8 mode of the source-free MTS, we found that it is the *x*-oriented currents (adjacent currents are opposite) on four corner patches that lead to radiation pattern bulge at four corners (Fig. 2 and Fig. 13), thus lowering boresight gain at this frequency.
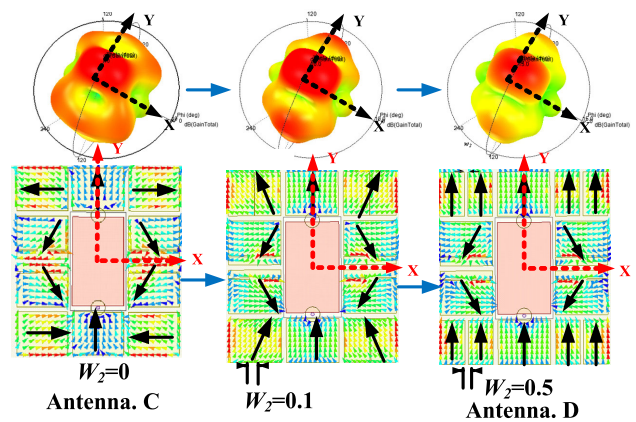

FIGURE 13. Evolution of longitudinal slots on corner patches.

Guided by the mode shifting method in [9], loading longitudinal (in the *y*-direction) slots at four corner patches can shorten the path of *x*-component currents, thus shifting the mode out of this frequency without affecting *y*-oriented J_1 mode. As indicated in Fig. 13, the *x*-component currents on four corner patches are gradually weakened to 0 (*y*-oriented current), as the longitudinal slots (w_2) becoming wider. As a result, the current distribution of the MTS gradually evolve from J_8 mode to modified J_9 mode whose out-of-phase currents have been suppressed, thus indicating the J_8 mode has been removed out from this frequency. Accordingly, the distorted radiation pattern is restored, the gain collapse is recovered and the in-band gain flatness is improved (Fig. 7(b)).

V. RESULTS AND DISCUSSION

In order to verify the reliability of our design, the proposed antenna was simulated, fabricated, assembled and measured. Fig. 14 shows the prototype of the proposed antenna.

As can be seen from Fig. 15, 51.4% simulated impedance bandwidth is realized (4.38-7.41 GHz), while the measured −10 dB impedance bandwidth is 50% (4.59-7.61 GHz). Because of the fluctuation of relative permittivity and
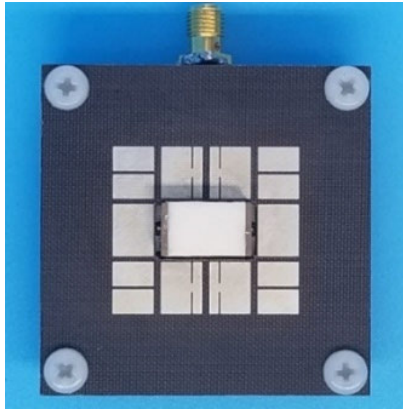
FIGURE 14. Prototype of proposed antenna.

manufacturing discrepancies, the resonant frequency and operating band of measured results are shifted to the higher side.

Fig. 15 shows the tendency of boresight gain over the operating band. In the lower frequency band, only DR radiates with a gain of 6 dBi. Then, beginning from 5.5 GHz, the broadside J_1 mode of the MTS leads to a rapid increase of boresight gain. With a series of arrangements of radiation restoration, the modified J_9 mode also contributes to gain enhancement, thus achieving a peak gain of 9 dBi. After that, gain drops dramatically due to the bandwidth limitation of the feeding network and radiation distortion of the MTS at higher order modes. Finally, a considerably even gain within 5-9 dBi over the operating band is obtained.
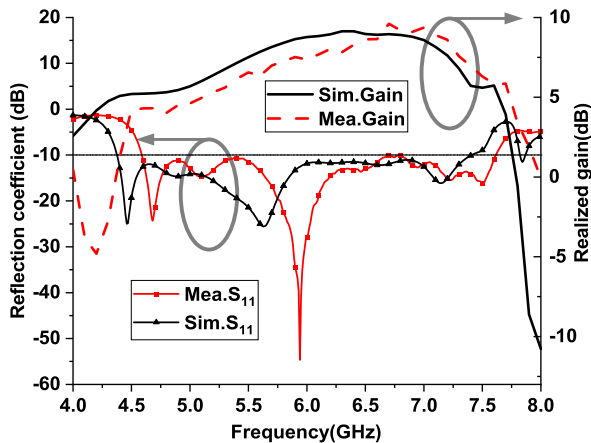

FIGURE 15. Simulated and measured reflection coefficient and realized gain of the proposed antenna.

Fig. 16 exhibits three typical radiation patterns that represent three working states at the low, middle and high frequency bands, respectively. At the low frequency, it is only the DR that radiates, which has a wider beam width comparing with middle frequency. In middle frequency band, the radiation is superimposed by $TE_{\delta 11}^x$ mode of DR and J_1 mode of the MTS, thus enhancing boresight gain with a slightly narrow beamwidth. In high frequency band, both DRA and modified J_9 mode of the MTS radiates with a slight

side lobe that has already been significantly improved. Additionally, stable broadside radiation, low cross-polarization level of -30 dB at boresight and reduced back radiation (a front-to-back ratio (FBR) of 15 dB) over operating band are obtained.
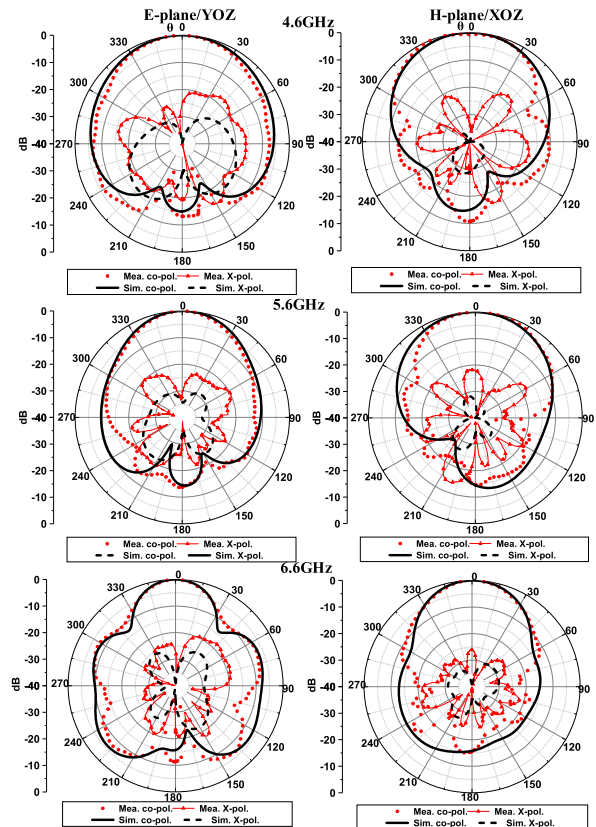

FIGURE 16. Simulated and measured radiation patterns.

Fig. 17 shows the simulated and measured radiation efficiency. Because the frequency shift toward the higher frequency band, the measured radiation efficiency at the high frequency band is higher than the simulated one. Meanwhile, an opposite phenomenon can be observed at the low frequency band. The above phenomenon observed in radiation efficiency (Fig. 17) is in accord with the tendency of the realized gain (Fig.15).

Compared with the slot coupled antennas [13]–[15], a 4-7dB reduced front-to-rear ratio (FBR) is obtained in our antenna due to the avoidance of grounded slot. Additionally, our design achieve a wider working bandwidth than [19] by reshaping the distorted HOM of the MTS for the wideband and broadside operation. Accordingly, this article introduces new modifications compared with [19] including four parts as follows: the differential feeding technique, loading transverse open-ended slots, loading longitudinal slots and shortening periodicity. Besides, in comparison of other antennas with a high FBR, our antenna has a wider working bandwidth. In summary, compared with other MAs in Table 1, the proposed antenna achieves a comparative wide bandwidth while preserving low back radiation.

TABLE 1. Comparison of The Proposed Antenna with Other Referenced prototypes.

Reference	Feeding	Size(λ_0^3)	Center frequency(GHz)	BW	FBR	Reshape HOM for wideband and broadside operation
[7]	Patch coupling	0.97×0.97×0.06	5.8	30%	20dB	No
[13]	Slot coupling	1.01×1.01×0.07	5.5	31%	11dB	No
[14]	Slot coupling	1.1×1.1×0.06	5.5	54%	11dB	No
[15]	Slot coupling	1.28×1.28×0.09	7.3	67.3%	8dB	No
[16]	Suspended dipole	0.73×0.73×0.08	5.5	24%	20dB	No
[17]	Coaxial probe	0.61×0.61×0.06	5.5	36%	20dB	No
[18]	Coplanar dipoles	1.02×1.02×0.11	5.1	45%	16dB	No
[19]	DR coupling	0.82×0.82×0.15	5.5	30%	15dB	No
Proposed	Differential DR coupling	1.02×1.02×0.17	5.9	51.4%	15dB	Yes

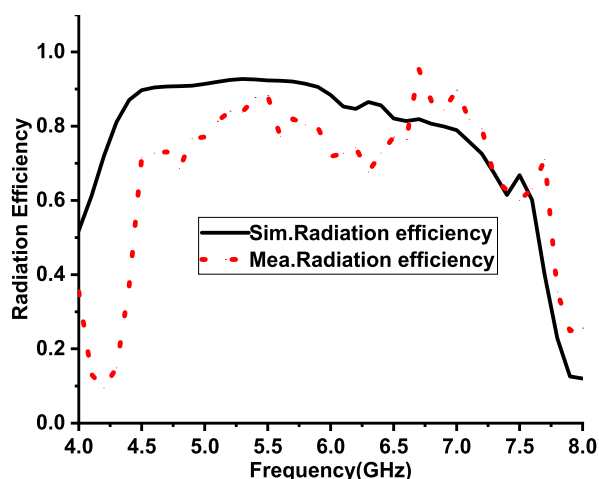*λ_0 is the wavelength in free space at the central operating frequency.

FIGURE 17. Simulated and measured radiation efficiency.

More importantly, a new method, reshaping the distorted HOM of the MTS for the broadside radiation, is presented in this article to further broaden the operating bandwidth. This newly introduced method of reshaping radiation patterns of HOM can also be further applied to other related designs for achieving various functional radiation.

VI. CONCLUSION
A DR fed wideband metasuface antenna is proposed, analyzed and experimentally verified in this article. The feeding source DR features stable excitation, low back radiation and high design flexibility. The $\text{TE}^x_{\delta 11}$ mode of the DR is combined with the J_1 and J_9 mode of the MTS, obtaining a multimode operation with wide bandwidth. By transforming the top-weak radiation pattern of the J_9 mode into the broadside radiation, a stable broadside performance within the wide band is achieved. The radiation reshaping methods are verified by using modal analysis and simulation, guiding the slot placement and patch size optimization for improving radiation pattern and gain stability. The simulated results agree well with the measured results, which indicate that a broad bandwidth, stable broadside radiation, low cross-polarization level and reduced back radiation are obtained in the proposed antenna.

REFERENCES
[1] K. D. Xu, J. Zhu, S. Liao, and Q. Xue, "Wideband patch antenna using multiple parasitic patches and its array application with mutual coupling reduction," *IEEE Access*, vol. 6, pp. 42497–42506, 2018.
[2] S. Feng, L. Zhang, H.-W. Yu, Y.-X. Zhang, and Y.-C. Jiao, "A single-layer wideband differential-fed microstrip patch antenna with complementary split-ring resonators loaded," *IEEE Access*, vol. 7, pp. 132041–132048, 2019.
[3] L. Chi, Z.-B. Weng, S. Meng, Y. Qi, J. Fan, W. Zhuang, and J. L. Drewniak, "Rugged linear array for IoT applications," *IEEE Internet Things J.*, vol. 7, no. 6, pp. 5078–5087, Jun. 2020.
[4] K. D. Xu, H. Xu, Y. Liu, J. Li, and Q. H. Liu, "Microstrip patch antennas with multiple parasitic patches and shorting vias for bandwidth enhancement," *IEEE Access*, vol. 6, pp. 11624–11633, 2018.
[5] L. Wang, Z. Weng, Y.-C. Jiao, W. Zhang, and C. Zhang, "A low-profile broadband circularly polarized microstrip antenna with wide beamwidth," *IEEE Antennas Wireless Propag. Lett.*, vol. 17, no. 7, pp. 1213–1217, Jul. 2018.
[6] Y.-X. Zhang, Y.-C. Jiao, L. Zhang, and J.-X. Wen, "Wideband 2-D monopulse antenna array with higher-order mode substrate integrated waveguide feeding and 3-D printed packaging," *IEEE Trans. Antennas Propag.*, vol. 68, no. 4, pp. 3259–3264, Apr. 2020.
[7] Z. Liang, J. Ouyang, and F. Yang, "Design and characteristic mode analysis of a low-profile wideband patch antenna using metasurface," *J. Electromagn. Waves Appl.*, vol. 32, no. 17, pp. 2304–2313, 2018.
[8] S. X. Ta and I. Park, "Low-profile broadband circularly polarized patch antenna using metasurface," *IEEE Trans. Antennas Propag.*, vol. 63, no. 12, pp. 5929–5934, Dec. 2015.
[9] H. L. Zhu, S. W. Cheung, K. Lun Chung, and T. I. Yuk, "Linear-to-circular polarization conversion using metasurface," *IEEE Trans. Antennas Propag.*, vol. 61, no. 9, pp. 4615–4623, Sep. 2013.
[10] B. A. Munk, *Frequency Selective Surfaces: Theory and Design*. New York, NY, USA: Wiley, 2000.
[11] Y.-X. Zhang, Y.-C. Jiao, Z. Zhang, and S. Feng, "Wideband accurate-out-of-phase-fed circularly polarized array based on penta-mode aperture antenna element with irregular cavity," *IEEE Trans. Antennas Propag.*, vol. 67, no. 1, pp. 638–642, Jan. 2019.
[12] P. Wang, Q. Wu, R.-B. He, and Y. Shao, "Design of low profile and wideband end-fire antenna using metasurface," *IEEE Access*, vol. 8, pp. 35752–35758, 2020.
[13] F. H. Lin and Z. N. Chen, "Low-profile wideband metasurface antennas using characteristic mode analysis," *IEEE Trans. Antennas Propag.*, vol. 65, no. 4, pp. 1706–1713, Apr. 2017.
[14] D. Chen, W. Yang, W. Che, and Q. Xue, "Broadband stable-gain multiresonance antenna using nonperiodic square-ring metasurface," *IEEE Antennas Wireless Propag. Lett.*, vol. 18, no. 8, pp. 1537–1541, Aug. 2019.
[15] J. Wang, H. Wong, Z. Ji, and Y. Wu, "Broadband CPW-fed aperture coupled metasurface antenna," *IEEE Antennas Wireless Propag. Lett.*, vol. 18, no. 3, pp. 517–520, Mar. 2019.
[16] F. H. Lin and Z. N. Chen, "A method of suppressing higher order modes for improving radiation performance of metasurface multiport antennas using characteristic mode analysis," *IEEE Trans. Antennas Propag.*, vol. 66, no. 4, pp. 1894–1902, Apr. 2018.

[17] F. H. Lin and Z. N. Chen, "Probe-fed broadband low-profile metasurface antennas using characteristic mode analysis," in *Proc. 6th Asia–Pacific Conf. Antennas Propag. (APCAP)*, Xi'an, China, Oct. 2017, pp. 664–666.

[18] F. H. Lin and Z. N. Chen, "Truncated impedance sheet model for low-profile broadband nonresonant-cell metasurface antennas using characteristic mode analysis," *IEEE Trans. Antennas Propag.*, vol. 66, no. 10, pp. 5043–5051, Oct. 2018.

[19] F. H. Lin and Z. N. Chen, "DRA-fed broadband metasurface antennas using characteristic mode analysis," in *Proc. 6th Asia–Pacific Conf. Antennas Propag. (APCAP)*, Xi'an, China, 2019, pp. 1–3.

[20] X. Yang, Y. Liu, and S.-X. Gong, "Design of a wideband omnidirectional antenna with characteristic mode analysis," *IEEE Antennas Wireless Propag. Lett.*, vol. 17, no. 6, pp. 993–997, Jun. 2018.

[21] C. Zhao and C.-F. Wang, "Characteristic mode design of wide band circularly polarized patch antenna consisting of H-shaped unit cells," *IEEE Access*, vol. 6, pp. 25292–25299, 2018.

[22] B. Feng, X. He, J.-C. Cheng, and C.-Y.-D. Sim, "Dual-wideband dual-polarized metasurface antenna array for the 5G millimeter wave communications based on characteristic mode theory," *IEEE Access*, vol. 8, pp. 21589–21601, 2020.

[23] K. S. Sultan, H. H. Abdullah, E. A. Abdallah, and H. S. El-Hennawy, "Metasurface-based dual polarized MIMO antenna for 5G smartphones using CMA," *IEEE Access*, vol. 8, pp. 37250–37264, 2020.

[24] A. Petosa, *Dielectric Resonator Antenna Handbook*. Norwood, MA, USA: Artech House, 2007.

[25] Y. Chen and C. Wang, *Characteristics Modes Theory and Applications in Antenna Engineering*. Hoboken, NJ, USA: Wiley, 2015.

[26] R. Harrington and J. Mautz, "Theory of characteristic modes for conducting bodies," *IEEE Trans. Antennas Propag.*, vol. 19, no. 5, pp. 622–628, Sep. 1971.

[27] R. Kumar Mongia and A. Ittipiboon, "Theoretical and experimental investigations on rectangular dielectric resonator antennas," *IEEE Trans. Antennas Propag.*, vol. 45, no. 9, pp. 1348–1356, Sep. 1997.

YONGHUI QIU received the B.S. degree in electronic engineering from the Xi'an University of Posts and Telecommunications, Xi'an, China, in 2018. He is currently pursuing the M.S. degree with Xidian University, Xi'an. His current research interests include dielectric resonator antenna, metasurface antenna, wideband antenna, and radiation pattern restoration.

ZIBIN WENG (Senior Member, IEEE) received the B.S. degree in electronic engineering and the Ph.D. degree in electromagnetic field and microwave technology from Xidian University, Xi'an, China, in 2004 and 2009, respectively. He is currently an Associate Professor with Xidian University. His current research interests include circularly polarized antennas, millimeter-wave antennas, and antenna arrays.

ZHI-QIANG ZHANG received the B.S. degree in electromagnetic field and microwave technology from Xidian University, Xi'an, China, in 2001, the M.S. degree from the Northwest Institute of Nuclear Technology (NINT), Xi'an, in 2004, and the Ph.D. degree in electromagnetic field and microwave technology from Xidian University, in 2014. Since 2004, he has been a Researcher with the High Power Microwave (HPM) and Antenna Research Group, NINT. His research interests include HPM wave propagation, radiation, and measurement.

JIANFENG LIU received the B.S. degree in electronic engineering from Xidian University, Xi'an, China, in 2018, where he is currently pursuing the M.S. degree. His current research interests include radiation pattern diversity antenna, metasurface antenna, and microstrip antenna.

HONG-WEI YU received the B.S. degree in electrical engineering from Xidian University, Xi'an, China, in 2014, where he is currently pursuing the Ph.D. degree. His current research interests include microstrip antennas, circularly polarized antennas, leaky-wave antennas, and phased array.

YI-XUAN ZHANG (Graduate Student Member, IEEE) received the B.S. degree in electrical engineering from Xidian University, Xi'an, China, in 2017, where he is currently pursuing the Ph.D. degree with the National Key Laboratory of Antennas and Microwave Technology. His current research interests include optimization techniques, antenna and phased arrays, and array signal processing. He was a recipient of the Chinese National Graduate Scholarship in 2018 and 2019, and the Best Student Paper Award in the 2019 International Symposium on Antennas and Propagation (ISAP).

• • •